



ISSN: 0067-2904

Effects of Porous Media on the Convective Heat Transfer in Nanofluid-Based Photovoltaic/Thermal System

Hanan S. Alzamili^{1*}, Hazim H. Hussain¹, Raed Abed Mahdi²

¹ Department of Atmospheric Sciences, College of Science, Mustansiriyah University, Baghdad, Iraq

² Training and Energy Research Office, Ministry of Electricity, Baghdad, Iraq

Received: 11/9/2023

Accepted: 20/2/2024

Published: 28/2/2025

Abstract

The convective heat transfer and nanofluid flow through porous media within the Photovoltaic/Thermal system (PV/T) under maximum air temperatures of 10, 25, and 52 °C in Baghdad city were investigated numerically. The PV/T system was filled with porous media and nanofluid, where the porous media consisted of open-cell aluminum foam (6101-T6 alloy) with a pore density of 20 PPI and a porosity of 0.9353-0.92%. The nanofluids were composed of aluminum oxide (Al₂O₃) and silicon dioxide (SiO₂) nanoparticles suspended in water and ethylene glycol (EG) with a volume fraction of 1-3 % and a nanoparticle diameter of 25 nm. A high-efficiency solar panel with a thermal collector was used at tilt angles of 0°, 10°, 30°, 45°, and 90°. The Finite-Volume Method (FVM) was employed to solve the governing equations of momentum, continuity, and energy. The study examined the effects of porous media and nanofluid properties, as well as tilt angles, on the performance of the PV/T system. The findings indicate that the highest heat transfer coefficient was attained when employing Al₂O₃-water nanofluids and aluminum foam at a PV/T tilt angle of 90°. The heat transfer coefficient increased with the PV/T tilt angle, nanoparticle volume fraction, and Reynolds number, while it demonstrated a decrease with porosity. An increase in the Reynolds number from 600 to 1700 resulted in a 6% enhancement in the heat transfer coefficient. Conversely, an increase in porosity led to an approximate 1% decrease in the average heat transfer coefficients. Using water as the base fluid improved the heat transfer coefficient by 6% compared to EG. Additionally, as the tilt angle increased from 0° to 90°, the heat transfer coefficient experienced a 2.5% enhancement. The combination of nanofluid with aluminum foam improved the thermal efficiency compared to nanofluid and base fluids alone. Moreover, the thermal efficiency remained consistent with an increase in heat flux.

Keywords: Convection Heat Transfer, Photovoltaic/Thermal System, Nanofluids, Aluminium Foam, Porous Media.

تأثير الوسائط المسامية على انتقال الحرارة بالحمل الحراري في النظام الكهروضوئي/الحراري القائم على السوائل النانوية

حنان سعد الزامل^{1*}, حازم حمود حسين², رائد عبد مهدي³

* Email: hanansaad@uomustansiriyah.edu.iq

^{1,2} قسم علوم الغلاف الجوي، كلية العلوم، الجامعة المستنصرية، بغداد، العراق
³ دائرة التدريب وبحوث الطاقة، وزارة الكهرباء، بغداد، العراق

الخلاصة

تمت دراسة انتقال الحرارة بالحمل الحراري وتدفق الموائع النانوية عبر الوسائط المسامية ضمن النظام الكهروضوئي/الحراري (PV/T) في ظل الحد الأقصى لدرجة حرارة الهواء لمدينة بغداد 10، 25، و 52 درجة مئوية. تم ملئ نظام PV / T بالوسائط المسامية والسوائل النانوية، حيث تتكون الوسائط المسامية من رغوة الألومنيوم ذات الخلية المفتوحة (سبيكة T6-6101) بكثافة مسام تبلغ 20 PPI ومسامية 0.92-0.9353. تتكون السوائل النانوية من جسيمات نانوية من أكسيد الألومنيوم (Al_2O_3) وثاني أكسيد السيليكون (SiO_2) معلقة في الماء وجلايكول الإيثيلين (EG) بجزء حجمي يتراوح من 1-3 % و قطر جسيمات يبلغ 25 nm. تم استخدام الألواح الشمسية عالية الكفاءة مع المجمع الحراري بزوايا ميل 0، 10، 30، 45، و 90. تم استخدام طريقة الحجم المحدود (FVM) لحل المعادلات الحاكمة للزخم والاستمرارية والطاقة. تناولت الدراسة تأثيرات الوسائط المسامية وخصائص الموائع النانوية بزوايا الميل على أداء PV/T. تشير النتائج إلى أنه تم الحصول على أعلى معامل انتقال للحرارة عند استخدام المائع النانوي أظهرت (Al_2O_3 - الماء) ورغوة الألومنيوم بزوايا ميل لنظام PV/T قدرها 90°. أظهر معامل انتقال الحرارة زيادة مع زاوية ميل PV/T، ونسبة حجم الجسيمات النانوية، ورقم رينولدز، في حين أظهر انخفاضاً مع المسامية. أدت زيادة عدد رينولدز من 600 إلى 1700 إلى تحسين معامل انتقال الحرارة بنسبة 6%. على العكس من ذلك، أدت الزيادة في المسامية إلى انخفاض بنسبة 1% تقريباً في متوسط معامل نقل الحرارة. أدى استخدام الماء كسائل أساسي إلى تحسين معامل نقل الحرارة بنسبة 6% مقارنة بـ EG. بالإضافة إلى ذلك، مع زيادة زاوية الميل من 0° إلى 90°، شهد معامل نقل الحرارة تحسناً بنسبة 2.5%. أدى الجمع بين السائل النانوي ورغوة الألومنيوم إلى تحسين الكفاءة الحرارية مقارنةً بالسوائل النانوية والسوائل الأساسية وحدها. علاوة على ذلك، ظلت الكفاءة الحرارية متمسكة مع زيادة التدفق الحراري.

1. Introduction

The sun is the primary source of energy for the Earth, providing solar radiation in the form of electromagnetic radiation [1]. The power received from the sun on Earth is approximately 1.8×10^{11} MW/second [2]. Due to the increasing cost and environmental concerns associated with fossil fuels, there is a growing need for renewable energy sources [3, 4]. Global warming conditions cause a severe shortage of energy supply. As a result, renewable energy sources must be introduced [5]. Solar energy is one of the most abundant renewable energy sources and is considered significant in Iraq and worldwide [6,7]. Solar photovoltaic/thermal (PV/T) technology is widely used in all sectors since it generates thermal and electrical energy. However, maintaining the operating temperature of PV/T systems, especially in high-temperature regions, is a challenge [8]. The air temperature in Baghdad can reach a maximum of 52 °C during the summer, negatively affecting the performance of solar panels. It is crucial to minimize the operating temperature to ensure optimal efficiency [9]. By increasing the size of the heat exchanger, the thermal efficiency of the plant can be significantly improved. Various techniques can be used to improve the efficiency of thermal devices, which can be divided into two categories: active and passive [10]. One of the passive techniques that will be focused on is the improvement of the properties of heat transfer fluids (nanofluids). Nanofluids are fluids that contain suspended nanoparticles, such as metal and dioxide, in a base fluid. To enhance heat transfer, nanofluids can be employed because traditional heat transfer fluids have low thermal conductivity compared to nanofluids [11]. Another passive technique is the use of porous media, such as rocks or open-cell aluminum foams, which have interconnected voids within a solid matrix. Porous media offer advantages such as increased dissipation area and improved fluid mixing due to abnormal fluid flow around each bead [12].

Numerous studies have been conducted on a PV/T system with porous media and nanofluids. Mousavi et al. [13] studied numerically the thermal performance of a PV/T system combined with Phase Change Materials (PCMs) in a porous medium. Their results showed a thermal efficiency of 83% when using Paraffin C22 as the storage material and a mass flow rate of 0.02 kg/s. Cui and Zhu [14] investigated experimentally the influence of utilizing Mg-water nanofluid with different concentrations of 2, 6 and 10 % on the efficiency of the PV/T system. Their results indicated a total efficiency beyond 60%. Alsalame et al. [15] studied experimentally the performance assessment of the PV/T system utilizing CuO/water and Al₂O₃/water nanofluids. Based on their findings, utilizing nanofluids as a heating medium in the system enhanced the efficiency compared to conventional heating media. Gelis et al. [16] investigated experimentally the impacts of nanofluids on the electrical and thermal efficiency of a PV/T system. Their outcomes detected that the thermal and electrical efficiency of the PV/T system improved after adding the nanofluids.

The utilization of porous media and nanofluids to improve the efficiency of PV/T systems has been identified as an important and intriguing topic in the existing literature. This article presents a numerical simulation of convection heat transfer within a Photovoltaic/Thermal (PV/T) system, with nanofluid flow through a porous structure made of open-cell aluminum foam, focusing on the maximum air temperatures experienced during the different seasons in Baghdad.

2. Material and Method

2.1 Physical Description of the Problem

A porous media inserted inside a two-dimensional rectangular channel was studied. The top part of the rectangular channel features a high-efficiency solar panel (JKM465M-7RL3-V Jink solar brand) with a length of 2182 mm. The working fluid enters the PV/T collector with a fully developed flow velocity (u_{∞}) and a temperature of $T_{\infty}=300$ K, as shown in Figure 1. The convective heat transfer and fluid flow within the nanofluid-filled aluminum foam are influenced by several factors, including the tilt angle of the PV/T system, the volume fraction of nanoparticles, the Reynolds number (Re), and the porosity of the porous media. These factors were investigated in this study under the following criteria:

1. A constant heat flux of 833 W/m² at the upper wall to simulate the solar radiation with the no-slip condition.
2. Maximum Baghdad city air temperatures of 10, 25, and 52°C
3. Aluminum foam with a porosity of 0.9353-0.92% and a pore density of 20 PPI.
4. Different base nanofluid types of ethylene glycol and water with SiO₂ and Al₂O₃ nanoparticles of 1, 2, and 3 % volume fractions.
5. Reynolds numbers ranging from 600 to 1700.
6. The tilt angles of the PV/T system ranging from 0°-90°.

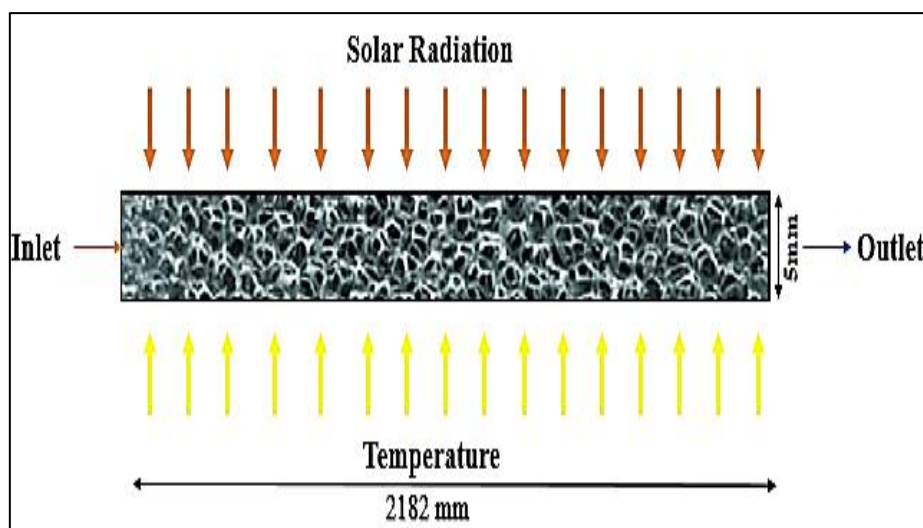


Figure 1: 2D numerical model of the PV/T system

Data obtained from the weather station of Mustansiriyah University revealed that the worst weather conditions in Baghdad were on June 21st of each year, resulting in a heat flux of approximately 833 W/m^2 . This measurement provides insight into the intensity of heat experienced in Baghdad during this particular period [17].

2.2 Assumption

Some assumptions were made to simplify the problem:

1. The flow was assumed to be in a steady state, two-dimensional, and incompressible with a fully developed laminar regime.
2. Internal heat creation, chemical reactions, and viscous dissipation were not considered.
3. The fluid's thermophysical properties remained constant at 300 K temperature.
4. The isotropic, homogenous aluminum foam was a solid matrix in local equilibrium with a single-phase fluid that was saturated with it.
5. The aluminum foam permeability values were considered constant for all fluids used at each porosity.
6. In the Brinkman viscous term, effective viscosity was equal to fluid viscosity.
7. Solar panel and thermal collector thickness were considered negligible.
8. Heat flux was constant (833 W/m^2) with PV/T collector angles.

2.3 Governing Equations

Darcy-Forchheimer's model was used to simulate the flow and incorporate the effect of inertia in the area of the aluminum foam as [18]:

$$-\nabla p = \underbrace{\frac{\mu}{K} \vec{v}}_{\text{Darcy's term}} + \underbrace{\frac{\rho C_f}{\sqrt{K}} |v| v_j}_{\text{Forchheimer's term}} \quad (1)$$

The equations of energy, Navier-Stokes, and continuity were used to model the fluid domain.

Continuity:

$$\nabla \cdot (\rho \vec{v}) = 0 \quad (2)$$

Momentum:

$$\nabla \cdot (\rho \vec{v}) = -\nabla p + \nabla \cdot \bar{\bar{\tau}} + \rho \vec{g} + \vec{F} \quad (3)$$

Where: p = static pressure, \bar{t} = stress tensor, and $\rho\vec{g}$ and \vec{F} = gravitational body force and the external body forces, respectively. The vector \vec{F} also encompasses additional model-dependent source terms such as porous media. The stress tensor \bar{t} is given by [18]:

$$\bar{t} = \mu \left[(\nabla\vec{v} + \nabla\vec{v}^T) - \frac{2}{3}\nabla\cdot\vec{v}I \right] \quad (4)$$

Where: μ = molecular viscosity, and I = the unit tensor. ANSYS FLUENT software was used to solve the momentum and continuity conservation equations in a porous region with the assumption of isotropic porous media porosity ε and single phase flow, as follows [19]:

Continuity:

$$\nabla\cdot(\varepsilon\rho\vec{v}) = 0 \quad (5)$$

Momentum:

$$\nabla\cdot(\varepsilon\rho\vec{v}) = -\varepsilon\nabla P + \nabla\cdot(\varepsilon\bar{t}) + \varepsilon\rho\vec{g} + \vec{F} \quad (6)$$

\vec{F} are a summation of the gravitational external body forces and body force, which accounts for fluid losses due to viscous and inertial forces inside porous media. FLUENT describes it as follows:

$$F_i = - \left(\underbrace{\sum_{j=1}^3 D_{ij}\mu v_j}_{\text{viscous resistance term or Darcy's term}} + \underbrace{\sum_{j=1}^3 C_{ij}\frac{1}{2}\rho|v|v_j}_{\text{inertial resistance term or Forchheimer term}} \right) \quad (7)$$

Where: F_i = the i^{th} momentum equation's external body force term, D = viscous resistance, and C = inertial resistance. Assuming that the effective viscosity is equal to the fluid viscosity in the Brinkman viscous term, FLUENT defines the axial pressure drops within the uniform matrix with just a steady flow and without internal axial body forces as follows [19]:

$$\frac{\partial(\varepsilon p)}{\partial x} = - \underbrace{\frac{\partial}{\partial x}(\varepsilon\rho v_i v_i)}_{\text{Convective acceleration}} + \underbrace{\frac{\partial(\varepsilon\tau_i)}{\partial x}}_{\substack{\text{Viscous stress also called} \\ \text{Brinkman viscous term or} \\ \text{bounding surface effect}}} + \varepsilon\rho\vec{g} - \left(\underbrace{\frac{D\mu v_i}{\text{Darcy's term}}}_{\text{Darcy's term}} + \underbrace{\frac{C}{2}\rho|v|v_i}_{\text{Forchheimer's term}} \right) \quad (8)$$

A comparison among Equations 1 to 8 demonstrates that the permeability in Darcy's term is related to the term of viscous resistance in Equation 7 by the following expression:

$$D = \frac{1}{K} \quad (9)$$

Permeability and the Forchheimer coefficient, via the Forchheimer term, are connected to the term of inertial resistance by the following relationship:

$$C = \frac{2c_f}{\sqrt{K}} \quad (10)$$

Energy equation:

In porous media, the local thermal equilibrium between the solid phase and the fluid is presumed. Consequently, the energy equation assumes the following form:

Fluid region:

$$\frac{\partial}{\partial x}(\varepsilon\rho_f E_f + (1-\varepsilon)\rho_s E_s) + \nabla\cdot(\vec{v}(\rho_f E_f + p)) = \nabla\cdot(k\nabla T - \sum_j h_j J_j + (\bar{t}\cdot\vec{v})) + S_f^h \quad (11)$$

Porous region:

$$\frac{\partial}{\partial x} (\epsilon \rho_f E_f + (1 - \epsilon) \rho_s E_s) + \nabla \cdot (\vec{v} (\rho_f E_f + p)) = \nabla \cdot (k_{eff} \nabla T - \sum_j h_j J_j + (\bar{\tau} \cdot \vec{v})) + S_f^h \quad (12)$$

Where: E_f = total fluid energy, E_s = total solid media energy, k_{eff} = effective thermal conductivity of the media, S_f^h = fluid enthalpy source term, and J_j = diffusion flux of species i .

FLUENT uses the volume-averaged conductivity of the fluid and the solid conductivity to calculate the effective thermal conductivity in a porous media k_{eff} [20]:

$$k_{eff} = \epsilon k_f + (1 - \epsilon) k_{porous\ media} \quad (13)$$

2.4 Governing Parameter

To calculate the thermal efficiency η_{th} of a PV/T system, the following equation was used [21]:

$$\eta_{th} = \frac{Q_u}{I} \quad (14)$$

Where: I = solar irradiance (W/m^2), and Q_u = useful thermal energy which was computed as follows:

$$Q_u = \dot{m} C_p (T_{out} - T_{in}) \quad (15)$$

Where: \dot{m} = mass flow rate, C_p = specific heat, and T_{out}, T_{in} = outlet and inlet temperature of the fluid, respectively.

2.5 Effective Thermophysical Properties of Nanofluids

The thermophysical characteristics of the nanofluids were determined using the equations provided in Table 1.

Table 1: Nanofluids thermophysical properties equations

Properties	Equation
Density [22]	$\rho_{nf} = \varphi \rho_{np} + (1 - \varphi) \rho_{bf}$
Specific Heat Capacity [23]	$C_{p,nf} = \varphi c_p + (1 - \varphi) c_{bf}$
Viscosity [24]	$\mu_{nf} = 1 / (1 - \varphi)^{2.5} \mu_{bf}$
Thermal Conductivity [25]	$k = k_{bf} [k_p + 2k_{bf} + 2\varphi(k_p - k_{bf})] / [k_p + 2k_{bf} - \varphi(k_p - k_{bf})]$

Where: φ is the volume fraction (%), bf is the base fluid, nf is the nanofluid, np is the nanoparticle. The thermophysical properties of nanoparticle material are summarized in Table 2.

Table 2: Thermophysical properties for nanoparticle material

Nanoparticles material	Density [kg/m3]	Specific heat [J/kg.K]	Thermal conductivity [W/m.K]
Al ₂ O ₃ [26]	3970	765	40
SiO ₂ [27]	2220	745	1.4

2.6 Thermophysical Properties of Aluminum Foam 6101-T6

Thermophysical properties of aluminum foam (alloy 6101-T6) were given by the following equations [28]:

$$\rho_{(al.f)} = (1 - \varepsilon)\rho_{(al.m.alloy\ 6101-T6)} \quad (16)$$

$$C_{P(al.f)} = (1 - \varepsilon)C_{P(al.m.alloy\ 6101-T6)} \quad (17)$$

$$k_{(al.f)} = (1 - \varepsilon)k_{(al.m.alloy\ 6101-T6)} * 0.33 \quad (18)$$

Where: *al.f* = is the aluminum foam and *al.m.alloy* = is the aluminum metal alloy. The factor 0.33 is the coefficient indicating the foam structure geometric or tortuosity factor. The thermophysical characteristics of used aluminum metal alloy 6101-T6 are listed in Table 3. The porous properties of aluminum foams are listed in Table 4.

Table 3: Thermophysical characteristics for aluminum metal alloy 6101-T6 [22]

Density [kg/m ³]	Specific heat [J/kg.K]	Thermal conductivity [W/m.K]
2700	895	218

Table 4: Porous properties of the aluminum foam alloy 6101-T6 samples [28]

Porous characteristics	Pore Density 20 PPI	
Porosity (ε) %	0.92	0.9353
Permeability (K) (m ²) *10 ⁻⁷	1.063	1.17
Inertia coefficient (C)	1.023e-01	9.82e-02

3. Simulation Model

3.1 Grid Independence Test

The two-dimensional model depicted in Figure 2 was constructed using a mesh for the fluid and aluminum foam zones. A grid independence test was conducted to achieve a grid with an optimal number of cells. Four different meshes with varying numbers of cells, were tested, and their results were compared. The purpose of this test was to assess the impact of the mesh used and the number of cells on the test results, intending to identify a mesh that would yield the most precise results in the shortest amount of time. As illustrated in Figure 3, it can be observed that for grids consisting of 399,367 cells, the heat transfer coefficient changes were negligible, amounting to less than 0.03%. Consequently, it can be concluded that a mesh comprising 399,367 cells produces the most accurate and reliable results.

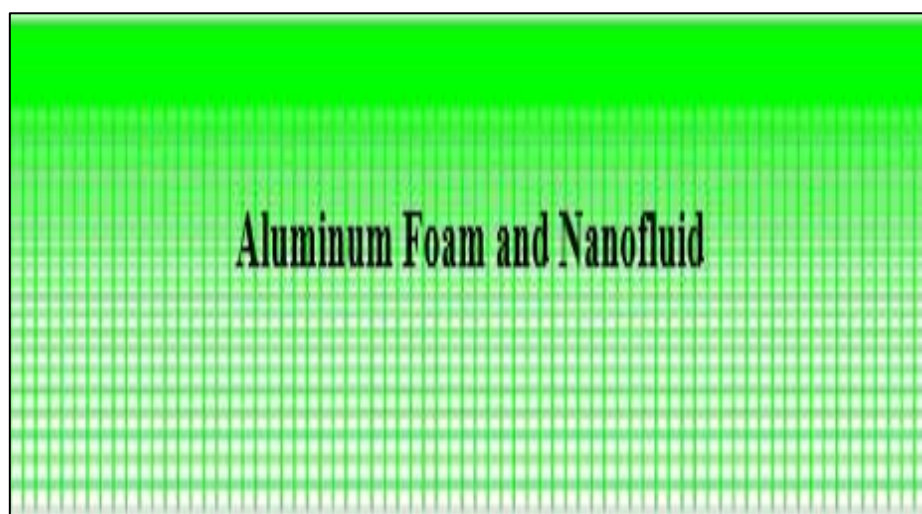


Figure 2: Computational model with mesh generation

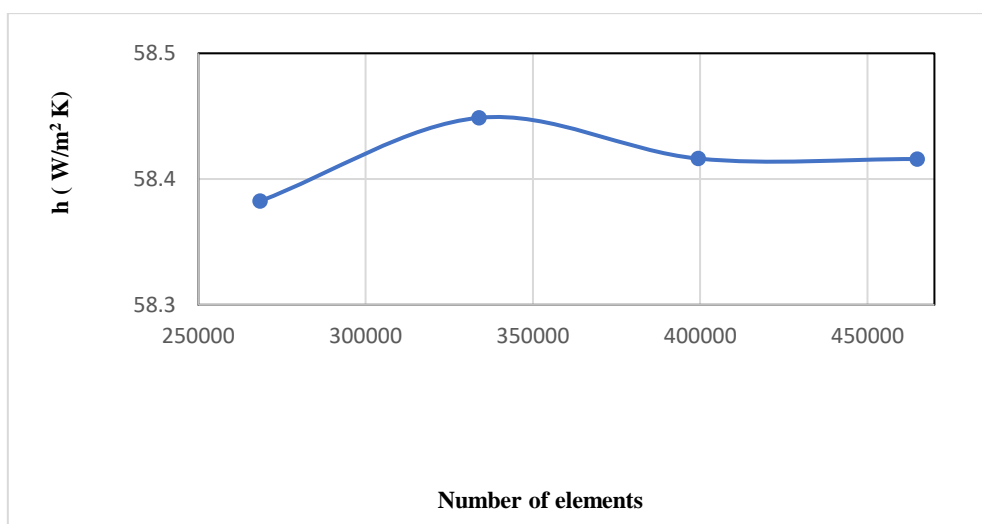


Figure 3: Comparison between heat transfer coefficient with several elements

3.2 Numerical and Modelling Settings

FLUENT was utilized to solve the energy and momentum equations for numerical analysis to understand the flow properties in the PV/T system. The pressure coupling and velocity problem were solved using the COUPLED algorithm. The second-order scheme was employed to find solutions to the pressure equations, while the second-order upwind scheme was used to find solutions to the energy and momentum equations. Convergence of the solutions for all variables was assumed when the normalized values of the residuals approached 10^{-6} .

4. Results and Discussions

4.1 Program Validation

There are very limited studies close to this work, so the outcomes were compared with fluid flow through porous media in a PV/T system, and the other with nanofluid flow through the PV/T system. The current results were compared with the results reached by Tahmasbi et al. [29], who studied a “2-dimensional PV/T system filled with porous metal foam”, and Karaaslan and Menlik [30], who studied “the heat transfer in a three-dimensional PV/T system”. The temperature was compared with the numerical results reported by them. The comparison reveals a 4% variance in the current results; see Figure 4 (a and b).

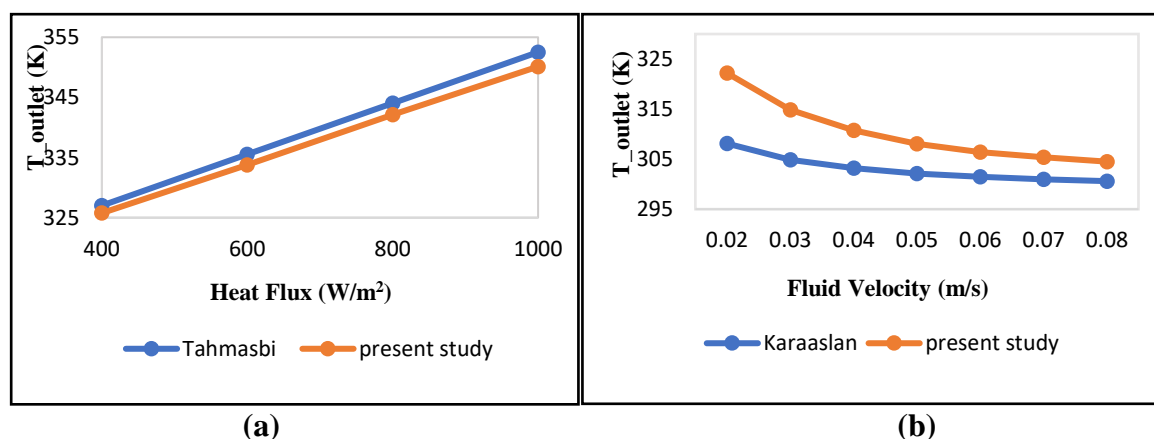


Figure 4: Evolution of the temperature in comparison with numerical results reported by (a) Tahmasbi et al. [29] (b) Karaaslan and Menlik [30]

4.2 Heat Transfer Coefficient

4.2.1 Porous Characteristics of the Aluminium Foam

The porosity of open-cell aluminum foam has a significant effect on the heat transfer coefficient. Figure 5 illustrates the relationship between the heat transfer coefficient and aluminum foam porosity. The PV/T back sheet was insulated, $\phi = 1\%$, $\Theta = 0^\circ$, $Re = 600$, $I = 833 \text{ W/m}^2$. The heat transfer coefficient values for the combination of aluminum foam with nanofluid, specifically Al_2O_3 -water+20 PPI, were found to be higher compared to those of the aluminum foam alone. When the porosity increased from 0.92 to 0.9353, the average heat transfer coefficients of the aluminum foam, SiO_2 -water+20 PPI, and Al_2O_3 -water+20 PPI decreased by 1.13 %, 1.14%, and 1.12% ($\text{W/m}^2 \text{ K}$), respectively. This reduction can be attributed to a decrease in thermal conductivity and specific heat with increasing porosity. Additionally, the heat transfer coefficient increased as permeability decreased. These results agree with that of Zheng et al.[31].

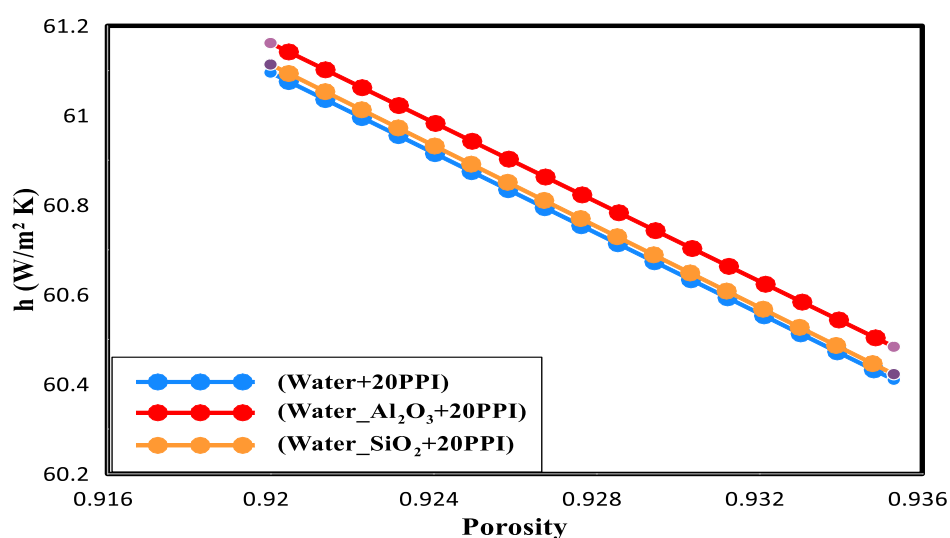


Figure 5: Effect of porosity on the heat transfer coefficient with and without nanofluid, $\Theta = 0^\circ$, $\phi = 1\%$, $Re = 600$

4.2.2 Base Fluid, Nanoparticles, and Reynolds Number Effects

Figure 6 presents the heat transfer coefficient values plotted against the Reynolds number for different types of base fluids and nanofluids. PV/T back sheet was insulated, $\phi = 1\%$, $\Theta = 0^\circ$, $Re = 600-1700$, $I = 833 \text{ W/m}^2$. When water was used as the base fluid, a higher heat transfer coefficient value than that using ethylene glycol was noted. The heat transfer coefficient with water was 6% higher than that with ethylene glycol, primarily due to the improved thermal conductivity of water. The heat transfer coefficient slightly increased when nanofluids were used due to the improvement of the fluid thermophysical properties compared to the base fluid. The greatest outcomes were attained with the nanofluid of water- Al_2O_3 compared with the water- SiO_2 nanofluids due to its enhanced thermophysical properties. The average heat transfer coefficient increased with an increase in Re due to the temperature and velocity gradients on the surface increasing with increasing Reynolds number. When Reynolds number increased from 600 to 1700, the heat transfer coefficient enhanced by 6%. These results were in good agreement with those of Saleh and Sundar [32].

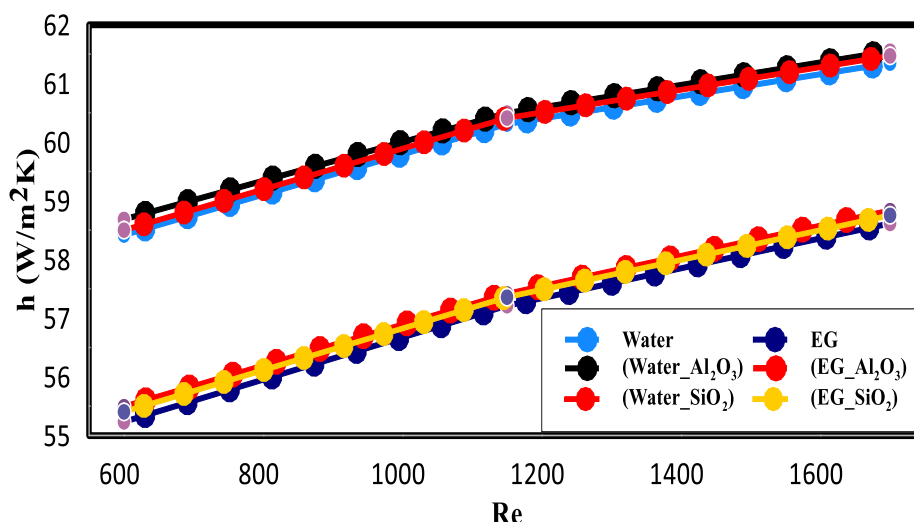


Figure 6: The effect of Re on heat transfer coefficient, $\phi = 1\%$, $\Theta = 0^\circ$

4.2.3 Nanoparticle Volume Fraction

Figure 7 shows the impact of water- Al_2O_3 and water- SiO_2 nanofluids with volume fractions of 1, 2, 3 % on the heat transfer coefficient. The PV/T back sheet was insulated, $\Theta = 0^\circ$, $\text{Re} = 600$, $I = 833 \text{ W/m}^2$. With increasing nanoparticle volume percentage, the heat transfer coefficient increased due to the improvement of the thermophysical properties. The highest amounts of the heat transfer coefficient were obtained with the water- Al_2O_3 nanofluid. These results were in acceptable agreement with the findings of Chadi et al. [33].

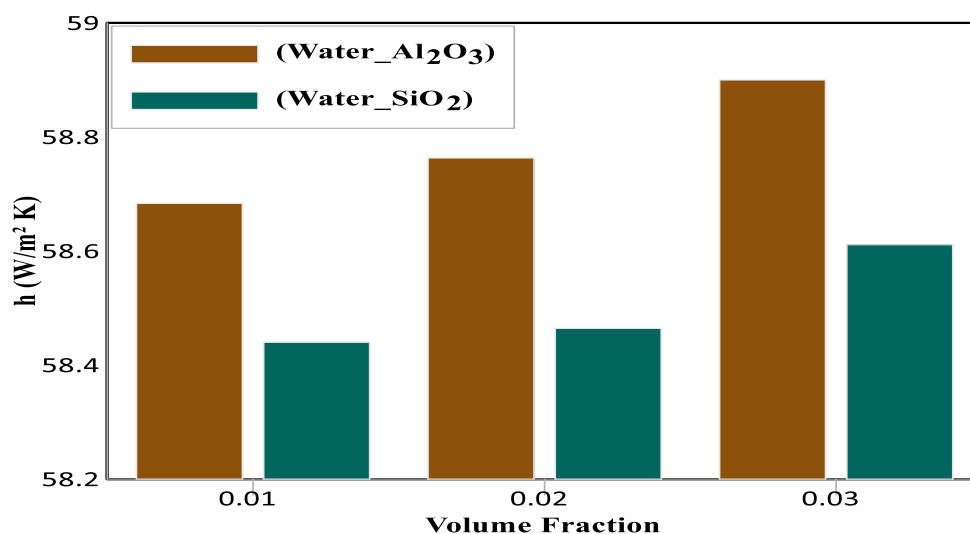


Figure 7: The impact of nanofluid's volume fraction on the heat transfer coefficient, $\text{Re} = 600$, $\Theta = 0^\circ$

4.2.4 PV/T System Tilt Angle

Figure 8 shows the heat transfer coefficient values for five different tilt angles of 0° , 10° , 30° , 45° , and 90° , with $I = 833 \text{ W/m}^2$, porosity = 0.92 %, and $\text{Re} = 600$. The PV/T back sheet was insulated. According to the findings, the heat transfer coefficient increased with the increase in the PV/T system inclination angle to 90° because there was a greatest temperature gradient and an improvement in the temperature distribution in the system. When the tilt angle increased from 0° to 90° , the heat transfer coefficient enhanced by 2.5%. These findings were a good qualitative acceptance of the findings of Hussain et al. [34].

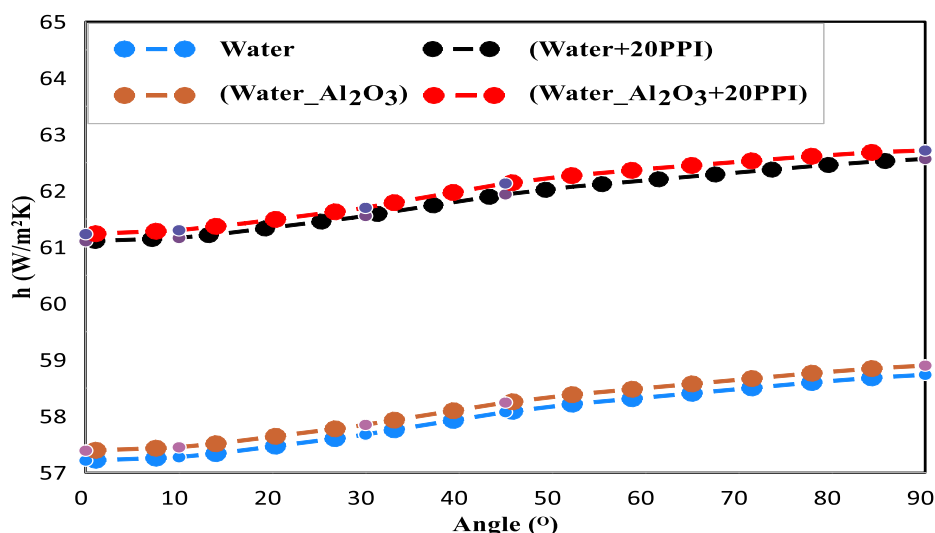


Figure 8: The impact of the tilt angle on the heat transfer coefficient, $\phi = 1\%$, porosity=0.92 %

4.2.5 Effect of Baghdad City Air Temperature on PV/T Performance

Figure 9 shows the effects of Baghdad city air temperature when the system was insulated and at the air temperature of 10, 25, and 52 °C on the heat transfer coefficient with water, water-Al₂O₃ nanofluid, aluminum foam with porosity of 0.92 %, and aluminum foam with nanofluid, $I=833 \text{ W/m}^2$. The heat transfer coefficient value was the best when the system was completely isolated. These findings were a good qualitative acceptance of the findings of Nahar et al.[35].

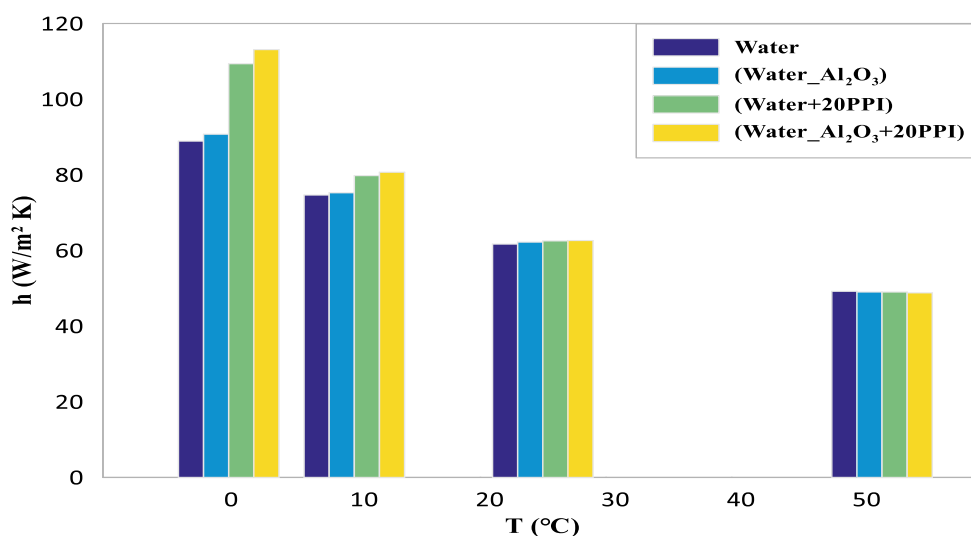


Figure 9: Impact of temperature on heat transfer coefficient, $\phi = 1\%$, $\Theta=0^\circ$

4.3 Thermal Efficiency of PV/T System

Figure 10 shows the thermal efficiency value versus solar radiation, with $Re=600$, PV/T tilt angle $=0^\circ$, $\phi = 1\%$, $I=833 \text{ W/m}^2$, porosity=0.92 %, and the PV/T back sheet was insulated. The efficiency remained the same when the solar radiation was raised due to the increase of the numerator and the denominator of Eq. (14) as the heat flux increased. As can be seen from the figure, thermal efficiency enhanced slightly with aluminum foam and both water-Al₂O₃+20 PPI and SiO₂-water+20 PPI compared with using nanofluid only. These findings were in good qualitative agreement with the results of Tahmasbi et al. [29] and Karaaslan and Menlik[30].

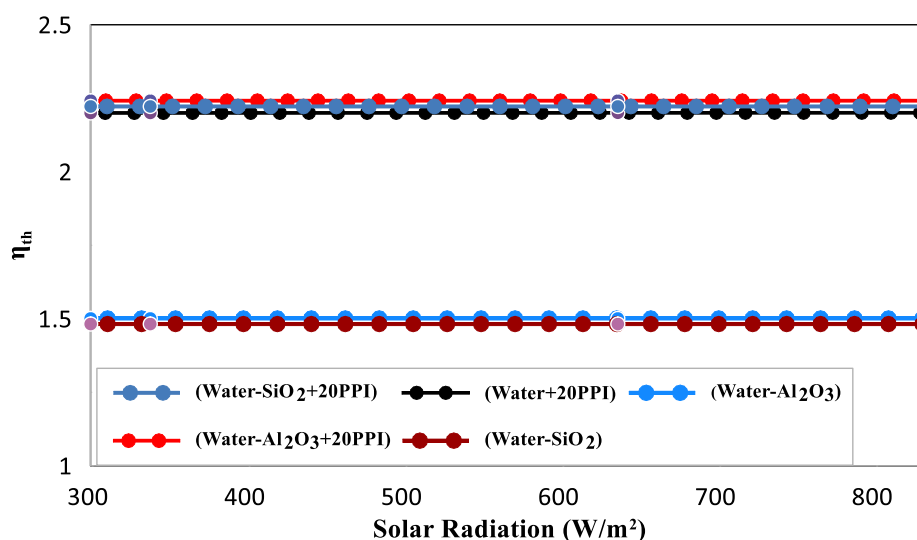


Figure 10: Variation of the thermal efficiency versus solar radiation, $\phi = 1\%$, $\Theta = 0^\circ$, $Re = 600$

5. Conclusions

In this study, a PV/T system filled with porous media and nanofluid was numerically investigated. The effects of the thermophysical characteristics of aluminum foam and nanofluid on the heat transfer coefficient were analyzed. The findings revealed that the heat transfer coefficient increased when nanofluid was used and further increased when aluminum foam was added. The highest heat transfer coefficient value was obtained with a pore density of 20 PPI and a porosity of 0.92 %. Among the nanofluids tested, Al₂O₃-water exhibited the highest heat transfer coefficient compared to SiO₂-water. The heat transfer coefficient increased with the PV/T tilt angle, nanoparticle volume fraction, and Reynolds number. Under the weather conditions of Baghdad City, the heat transfer coefficient was optimal when the system was fully insulated compared with the temperature degrees 10°, 25°, and 52 °C. Furthermore, the thermal efficiency remained constant even with an increase in solar radiation. The combination of aluminum foam and nanofluid showed an improved heat transfer coefficient compared to using nanofluid alone.

References

- [1] N. T. Ibraheem, H. H. Hussain, and O. L. Khaleed, "Modelling Heat Transfer in Solar Distiller with Additional Condenser Studying," *Al-Mustansiriyah Journal of Science*, vol. 32, no. 2, pp. 25-32, 2021.
- [2] O. A. Kreem and H. H. Hussain, "Performance of Elliptical Solar Cooker Suitable for Baghdad Environment," *Al-Mustansiriyah Journal of Science*, vol. 32, no. 4, pp. 1-5, 2021.
- [3] M. B. Al-hadithi and Y. M. Tayib, "Design and Performance Analysis of Spiral Solar Water Heater Using Iron Plate/Sand Absorber for Domestic Use," *Iraqi Journal of Science*, vol. 62, no. 11, pp. 4290-4299, 2021.
- [4] S. Serag and A. Echhelh, "Technical and Economic Evaluation of Electricity Generation and Storage Using Renewable Energy Sources on Socotra Island, Yemen," *Iraqi Journal of Science*, vol. 64, no. 6, pp. 2809-2842, 2023.
- [5] N. K. Kasim, H. H. Hussain, and A. N. Abed, "Enhancement of some electrical parameters of grid-connected PV solar system using planer concentrators," *Energy Sources, Part A: Recovery, Utilization, and Environmental Effects*, pp. 1-13, 2021.
- [6] A. R. Salih, "Seasonal Optimum Tilt Angle of Solar Panels for 100 Cities in the World," *Al-Mustansiriyah Journal of Science*, vol. 34, no. 1, pp. 104-110, 2023.
- [7] A. H. Ajil, "Evaluation and Comparison of Temperature-Based Models for The Prediction of The

- Monthly Average of Daily Global Solar Radiation for Baghdad City-Iraq," *Iraqi Journal of Science*, vol. 61, no. 3, pp. 533-539, 2020.
- [8] M. H. Alktrane, "A review of performance hybrid photovoltaic/thermal system for general-applications," *Hungarian Agricultural Engineering*, vol. 32, pp. 5-15, 2017.
- [9] M. Shojaeefard, N. Sakran, M. Sharfabadi, and N. Davoudi, "A Novel Review on Nano-fluid and Phase Change Material based Photovoltaic Thermal (PV/T) Systems," in *IOP Conference Series: Materials Science and Engineering*, vol. 1067, no. 1: IOP Publishing, p. 012099, 2021.
- [10] Y. H. Assaf, A. Akroot, H. A. Abdul Wahhab, W. Talal, M. Bdaiwi, and M. Y. Nawaf, "Impact of Nano Additives in Heat Exchangers with Twisted Tapes and Rings to Increase Efficiency: A Review," *Sustainability*, vol. 15, no. 10, p. 7867, 2023.
- [11] M. Awais et al., "Heat transfer and pressure drop performance of Nanofluid: A state-of-the-art review," *International Journal of Thermofluids*, vol. 9, p. 100065, 2021.
- [12] M. Habibishandiz and M. Saghir, "A critical review of heat transfer enhancement methods in the presence of porous media, nanofluids, and microorganisms," *Thermal Science and Engineering Progress*, vol. 30, p. 101267, 2022.
- [13] S. Mousavi, A. Kasaeian, M. B. Shafii, and M. H. Jahangir, "Numerical investigation of the effects of a copper foam filled with phase change materials in a water-cooled photovoltaic/thermal system," *Energy Conversion and Management*, vol. 163, pp. 187-195, 2018
- [14] Y. Cui and Q. Zhu, "Study of photovoltaic/thermal systems with MgO-water nanofluids flowing over silicon solar cells," in *2012 Asia-Pacific Power and Energy Engineering Conference*, IEEE, 2012, pp. 1-4.
- [15] H. A. Mahmood Alsalam, J. H. Lee, and G. H. Lee, "Performance Evaluation of a Photovoltaic Thermal (PVT) system using nanofluids," *Energies*, vol. 14, no. 2, p. 301, 2021.
- [16] K. Gelis, A. N. Celik, K. Ozbek, and O. Ozyurt, "Experimental investigation into efficiency of SiO₂/water-based nanofluids in photovoltaic thermal systems using response surface methodology," *Solar Energy*, vol. 235, pp. 229-241, 2022.
- [17] Mustansiriyah Uni. "Solar radiation data." <https://app.weathercloud.net/d1966703094#current> (accessed).
- [18] D. A. Nield and A. Bejan, *Convection in porous media*. Springer, 2006.
- [19] F. Ansys, "6.3 Tutorial Guide," *Fluent Inc*, 2006.
- [20] A. Fluent, "Fluent 14.0 user's guide," *Ansys Fluent Inc*, 2011.
- [21] A. L. Hernandez and J. E. Quiñonez, "Analytical models of thermal performance of solar air heaters of double-parallel flow and double-pass counter flow," *Renewable Energy*, vol. 55, pp. 380-391, 2013.
- [22] R. A. Mahdi, H. Mohammed, K. Munisamy, and N. Saeid, "Influence of various geometrical shapes on mixed convection through an open-cell aluminium foam filled with nanofluid," *Journal of Computational and Theoretical Nanoscience*, vol. 11, no. 5, pp. 1275-1289, 2014.
- [23] M. Jamei et al., "On the specific heat capacity estimation of metal oxide-based nanofluid for energy perspective—A comprehensive assessment of data analysis techniques," *International Communications in Heat and Mass Transfer*, vol. 123, p. 105217, 2021.
- [24] M. Klazly and G. Bognár, "A novel empirical equation for the effective viscosity of nanofluids based on theoretical and empirical results," *International Communications in Heat and Mass Transfer*, vol. 135, p. 106054, 2022.
- [25] R. A. Raja, J. Sunil, M. Hamilton, and J. Davis, "Estimation of thermal conductivity of nanofluids using theoretical correlations," *Int. J. Appl. Eng. Res.*, vol. 13, no. 10, pp. 7932-7936, 2018.
- [26] Y.-j. Hwang et al., "Stability and thermal conductivity characteristics of nanofluids," *Thermochimica Acta*, vol. 455, no. 1-2, pp. 70-74, 2007.
- [27] J. Koo and C. Kleinstreuer, "A new thermal conductivity model for nanofluids," *Journal of Nanoparticle research*, vol. 6, pp. 577-588, 2004.
- [28] R. A. Mahdi, H. Mohammed, and K. Munisamy, "The effect of various open cell aluminium foam

- geometrical shapes on combined convection heat transfer with nanofluid," vol. 3, pp. 615-629, 2013.
- [29] M. Tahmasbi, M. Siavashi, A. M. Norouzi, and M. H. Doranehgard, "Thermal and electrical efficiencies enhancement of a solar photovoltaic-thermal/air system (PVT/air) using metal foams," *Journal of the Taiwan Institute of Chemical Engineers*, vol. 124, pp. 276-289, 2021.
- [30] I. Karaaslan and T. Menlik, "Numerical study of a photovoltaic thermal (PV/T) system using mono and hybrid nanofluid," *Solar Energy*, vol. 224, pp. 1260-1270, 2021.
- [31] B. Zheng, Y. Liu, L. Zou, and R. Li, "Heat transfer characteristics of calcined petroleum coke in waste heat recovery process," *Mathematical Problems in Engineering*, vol. 2016, no. 5, pp 1-9, 2016.
- [32] B. Saleh and L. S. Sundar, "Thermal efficiency, heat transfer, and friction factor analyses of MWCNT+ Fe₃O₄/water hybrid nanofluids in a solar flat plate collector under thermosyphon condition," *Processes*, vol. 9, no. 1, p. 180, 2021.
- [33] K. Chadi, N. Belghar, B. Guerira, and A. Messaoudi, "Three-dimensional numerical study of thermal exchanges in different geometry sections of mini-channels using three different nanoparticles," *Metallurgical and Materials Engineering*, vol. 26, no. 1, pp. 103-119, 2020.
- [34] S. Hussain, K. Mehmood, M. Sagheer, and A. Farooq, "Entropy generation analysis of mixed convective flow in an inclined channel with cavity with Al₂O₃-water nanofluid in porous medium," *International Communications in Heat and Mass Transfer*, vol. 89, pp. 198-210, 2017.
- [35] A. Nahar, M. Hasanuzzaman, and N. Rahim, "A 3D comprehensive numerical investigation of different operating parameters on the performance of a PVT system with pancake collector," *Journal of Solar Engineering ASME*, vol. 55, pp. 245-266, 2017.